Title

Dysregulation of astrocyte extracellular signaling in Costello syndrome

Journal

Science Translational Medicine, 7(286)

ISSN

1946-6234

Authors

Krencik, Robert

Hokanson, Kenton C

Narayan, Aditi R

et al.

Publication Date

2015-05-06

DOI

10.1126/scitranslmed.aaa5645

Peer reviewed

HHS Public Access

Author manuscript

Sci Transl Med. Author manuscript; available in PMC 2015 June 19.

Published in final edited form as:

Sci Transl Med. 2015 May 6; 7(286): 286ra66. doi:10.1126/scitranslmed.aaa5645.

Dysregulation of astrocyte extracellular signaling in Costello syndrome

Robert Krencik[1], **Kenton C. Hokanson**[2], **Aditi R. Narayan**[1], **Jill Dvornik**[1], **Gemma E. Rooney**[1], **Katherine A. Rauen**[3], **Lauren A. Weiss**[4], **David H. Rowitch**[5], and **Erik M. Ullian**[1,6,*]

[1]Department of Ophthalmology, University of California, San Francisco, San Francisco, CA 94143, USA

[2]Neuroscience Program, University of California, San Francisco, San Francisco, CA 94143, USA

[3]Department of Pediatrics, University of California, Davis, Sacramento, CA 95817, USA

[4]Department of Psychiatry and Institute for Human Genetics, University of California, San Francisco, San Francisco, CA 94143, USA

[5]Department of Pediatrics, Eli and Edythe Broad Institute for Regenerative Medicine and Stem Cell Research, and Howard Hughes Medical Institute, University of California, San Francisco, San Francisco, CA 94143, USA

[6]Department of Physiology, University of California, San Francisco, San Francisco, CA 94143, USA

Abstract

Astrocytes produce an assortment of signals that promote neuronal maturation according to a precise developmental timeline. Is this orchestrated timing and signaling altered in human neurodevelopmental disorders? To address this question, the astroglial lineage was investigated in two model systems of a developmental disorder with intellectual disability caused by mutant Harvey rat sarcoma viral oncogene homolog (HRAS) termed Costello syndrome: mutant HRAS human induced pluripotent stem cells (iPSCs) and transgenic mice. Human iPSCs derived from patients with Costello syndrome differentiated to astroglia more rapidly in vitro than those derived from wild-type cell lines with normal HRAS, exhibited hyperplasia, and also generated an abundance of extracellular matrix remodeling factors and proteoglycans. Acute treatment with a farnesyl transferase inhibitor and knockdown of the transcription factor SNAI2 reduced expression of several proteoglycans in Costello syndrome iPSC-derived astrocytes. Similarly, mice in which

*Corresponding author. UllianE@vision.ucsf.edu.

Author contributions: R.K., K.A.R., L.A.W., D.H.R., and E.M.U. designed the study; K.C.H. conducted electrophysiology and subsequent data analysis; R.K. and A.R.N. conducted Western blots and RGC purification; R.K. and J.D. optimized and performed RT-qPCR;G.E.R. generated and characterized the iPSC lines and co-observed early S100B expression; L.A.W. and K.A.R. collected the fibroblast samples; R.K. supervised all experiments, carried out all additional experiments, and analyzed data; R.K., K.C.H., D.H.R., and E.M.U. co-wrote the paper.

Competing interests: The authors declare that they have no competing interests.

Data and materials availability: The raw and normalized microarray data have been deposited in National Center for Biotechnology Information's (NCBI's) Gene Expression Omnibus (GEO) and are accessible through GEO series accession number GSE64194.

SUPPLEMENTARY MATERIALS

www.sciencetranslationalmedicine.org/cgi/content/full/7/286/286ra66/DC1

mutant HRAS was expressed selectively in astrocytes exhibited experience-independent increased accumulation of perineuronal net proteoglycans in cortex, as well as increased parvalbumin expression in interneurons, when compared to wild-type mice. Our data indicate that astrocytes expressing mutant HRAS dysregulate cortical maturation during development as shown by abnormal extracellular matrix remodeling and implicate excessive astrocyte-to-neuron signaling as a possible drug target for treating mental impairment and enhancing neuroplasticity.

INTRODUCTION

Astrocytes are the most abundant neuroepithelium-derived cells in the central nervous system, and they serve many important roles for brain function. Notably, they are implicated in regulating cognition by means of neuronal synaptic remodeling and maintaining homeostasis of extrasynaptic ions and transmitters (1, 2). Little is known about how astrocytes are altered in neurodevelopmental disorders (NDDs) such as Rett syndrome, Fragile X syndrome, autism spectrum disorders, and genetic mutations of the Ras/mitogen-activated protein kinase (MAPK) pathway (3, 4). The cognitive and social dysfunction of NDDs are thought to be a result of changes in neuronal synapse formation and function, as well as disrupted timing of experience-dependent critical periods (5–7); however, it is not clear whether human astrocytes are specifically involved in these disease phenotypes. Do astrocytes direct the timing or function of cortical maturation and plasticity? One intriguing general hypothesis for NDD etiology is that an imbalance between neurogenesis and gliogenesis or an alteration in astrocyte functional properties disrupts the emergence of human astrocyte–generated extracellular signals that are crucial regulators of neuronal synapse formation, maturation, and pruning (8–13).

Cellular pathologies caused by disease-specific genetic background as well as identification of treatment targets can be investigated in human induced pluripotent stem cells (iPSCs) (14, 15). The use of patientderived iPSCs has revealed aberrations in several diseases involving astrocytes, including reduced synaptic function of neurons exposed to astrocytes (16–19). One common group of genetic NDDs—comprising neurofibromatosis 1 (NF1), LEOPARD syndrome, Legius syndrome, Noonan syndrome, cardiofaciocutaneous syndrome, and Costello syndrome (CS)—are caused by alterations in Ras pathway signaling and thus are called RASopathies (20, 21). Within the central nervous system, altered Ras/MAPK signaling promotes early generation of astrocytes from rodent neural stem cells (22–27), yet these syndromes have not yet been explored with human iPSC–derived astrocytes. Although the phenotypes of the various RASopathies can involve different tissues, these diseases share common symptoms in the nervous system, including neurocognitive impairment, macrocephaly, tumors, and autism-like traits (28–31).

Here, we have investigated properties of human astroglial cells harboring a RASopathy mutation to uncover cellular mechanisms that could lead to altered brain circuit function. We focused on CS (OMIM#218040) (32, 33), caused by hyperactivated Ras signaling resulting from mutations in Harvey rat sarcoma viral oncogene homolog (HRAS) (34), subsequently affecting a multitude of upstream and downstream signaling pathways (35). CS is most commonly the result of a spontaneous germline heterozygous glycine-to-serine

missense mutation at amino acid 12 ($HRAS^{G12S}$). This mutation initiates a relatively homogeneous clinical phenotype: psychomotor delay with low scores on intelligence and developmental indices (36). We used iPSCs from $HRAS^{G12S}$ human subjects and HRAS wild-type control lines ($HRAS^{WT}$) to test for functional changes in astrocytes and then confirmed and expanded our findings in a transgenic mouse model.

RESULTS

Enhanced Ras-specific maturation and potency of human CS astroglial progenitors

We first determined whether the temporal development and basic properties of the $HRAS^{G12S}$ human astroglial lineage were altered in comparison to $HRAS^{WT}$ cells by using an in vitro model system. iPSCs were generated from four unrelated CS $HRAS^{G12S}$ patient fibroblast lines and three $HRAS^{WT}$ unrelated control cell lines (Fig. 1A). For iPSC generation, we used well-characterized, nonintegrating episomal plasmids to acutely express reprogramming factors to avoid viral-mediated mutagenesis (37). We generated neuroepithelial cells (n = 5 differentiation replicates from separate iPSC passages for each subject line) that displayed no obvious differences in their ability to form neural tube-like rosettes and low expression of several previously identified iPSC-derived astroglial markers [NFIA, S100B, GFAP (glial fibrillary acidic protein), and CD44] (38), as expected at this stage. Subsequently, each line was differentiated toward the astroglial lineage with dorsal forebrain regional identity in the presence of growth factors EGF (epidermal growth factor) and FGF2 (fibroblast growth factor 2) (38, 39) (Fig. 1, B and C, and fig. S1).

We tested whether the mutant HRAS allele altered the general characteristics of human astroglia. Because there is no definitive set of criteria to identify human astroglial development, we used a panel of protein markers that have been shown to label this lineage in vitro and in vivo: S100, CD44, and GFAP (39, 40). The proportion of cells expressing these markers was compared in $HRAS^{G12S}$ and $HRAS^{WT}$ lines at three time points spanning development: weeks 8 (glial progenitors), 16 (mixed population), and 24 (astrocytes) of differentiation. During this period, $HRAS^{G12S}$ neuroglia more rapidly manifested a higher percentage of labeled cells than did the $HRAS^{WT}$ cells, suggesting accelerated development (Fig. 1, D and E). To generate an additional panel of astrocyte maturity markers, we compared mRNA $\log_2$ signals from $HRAS^{WT}$ cells at 8 and 28 weeks using microarray platforms, producing a list of consistently up-regulated transcripts (fig. S2). RT-qPCR analyses confirmed an $HRAS^{G12S}$-induced up-regulation of two of these potential astroglial markers: NFIA and thrombospodin 1 (THBS1). These findings demonstrate that the $HRAS^{G12S}$ mutation results in an acceleration of astroglial maturation. Nevertheless, this more rapid maturation was not apparent for all developmentally regulated genes, rather selectively affecting Ras-specific features (Fig. 1, F and G).

On the basis of evidence from previously described iPSC astroglial disease models, we also investigated whether the $HRAS^{G12S}$ cells exhibited signs of poor health by assessing cell death (17) and increased oxidation (16, 18). As expected, phosphorylated extracellular signal–regulated kinase (pERK), a marker of activated Ras signaling, was confirmed to be increased in $HRAS^{G12S}$ astroglia 24 hours after growth factor removal when compared to pERK in $HRAS^{WT}$ cells (Fig. 2A). In contrast, we saw no difference in the frequency of

glial progenitors undergoing apoptosis, as measured by presence of cleaved caspase 3 ($HRAS^{WT}$ = 3.7 ± 0.2%, $HRAS^{G12S}$ = 3.6 ± 0.6%) (Fig. 2B). We observed, in the near-homogeneous $HRAS^{G12S}$ astrocytes assayed at 24 weeks, a reduction in oxidative stress as determined by oxidation-induced probe fluorescence ($HRAS^{G12S}$ = 79 ± 8% of $HRAS^{WT}$ signal, P = 0.03; Fig. 2C). Because HRAS is known to modulate astrocyte proliferation (24), we characterized the rate of cell division. Astrocytes were dissociated and plated as a monolayer in the presence of continual treatment with the Ras pathway–activating growth factors FGF2 and EGF. $HRAS^{G12S}$ astrocytes exhibited increased proliferation during a 6-hour 5-bromo-2′-deoxyuridine (BrdU) pulse 1 day after plating (BrdU-positive percentages: $HRAS^{WT}$ = 28.3 ± 3.2%, $HRAS^{G12S}$ = 42.1 ± 1.9%, P = 0.003) (Fig. 2D). Likewise, there was an increase of proliferation measured after the removal of growth factors and addition of the maturation factor CNTF (ciliary neurotrophic factor) after 3 days (BrdU-positive percentages with a 12-hour pulse: $HRAS^{WT}$ = 4.5 ± 0.6%, $HRAS^{G12S}$ = 9.3 ± 2.0%, P = 0.016) (Fig. 2D). After 6 days without growth factors, proliferating cells were not detected in either group. These data implicate increased cell cycling of astrocyte progenitors as one cause of the observed early differentiation. In summary, human astroglia carrying the $HRAS^{G12S}$ mutation display early Ras-specific maturation and improved health across a broad array of assays.

Mutant HRAS expression, alterations in morphology, and diseased states have been linked to cellular senescence, and senescence may lead to changes in extracellular signaling (41–44). We examined $HRAS^{G12S}$ astrocytes 24 weeks after the start of differentiation for Ki67-labeling and β-galactosidase activity, two measurements of senescence (Ki67 decreases and the percent of cells with β-galactosidase activity increases in senescent cells). The percent of Ki67-labeled cells was not different between the lines ($HRAS^{WT}$ = 32.7 ± 1.8%, $HRAS^{G12S}$ = 31.8 ± 4.6%), and the percent of cells with β-galactosidase activity was lower in $HRAS^{G12S}$ cells ($HRAS^{WT}$ = 8.7 ± 0.5%, $HRAS^{G12S}$ = 6.6 ± 0.2%, P = 0.009) (Fig. 2, E and F). Together, the data indicate that the $HRAS^{G12S}$ cells do not undergo increased senescence at this stage of development.

As the two cell lines were maintained in culture, we observed morphological changes throughout the developmental timeline. Specifically, we observed a change in cell area quantified by sparse viral green fluorescent protein (GFP)–labeling of attached proliferating cells followed by area measurement after 1 week ($HRAS^{G12S}$/$HRAS^{WT}$ area average at 36 weeks after start of differentiation = 3.6, $P < 0.001$) (Fig. 2G). We next examined whether the morphological hypertrophy was an artifact of the in vitro culture systems. When cells were engrafted into mouse hippocampal organotypic slices, we noted that $HRAS^{G12S}$ astrocytes still exhibited a complex morphology in this alternate environment, including heightened maturation of traits such as increased volume and branching (Fig. 2H). Because CS human tissue was unavailable for study, we instead investigated astrocyte morphology in a transgenic mouse in which a flox-and-replace $HRAS^{G12V}$ allele was knocked into the endogenous HRAS locus (45). $HRAS^{G12S}$ mice do not currently exist. This line was crossed with a Blbp/Fabp7-Cre strain previously used in various models of RASopathies for robust recombination in the astroglial lineage (23, 25) and subsequently crossed with an Aldh1L1-GFP transgenic mouse to identify astrocytes. At postnatal day (p) 21, $HRAS^{G12V}$ mouse

astrocytes in the somatosensory cortex showed increased area, as measured by Aldh1L1-GFP signal (number of positive pixels: $HRAS^{WT}$ = 11,971 ± 438, $HRAS^{G12V}$ = 20,877 ± 1416, n = 45 cells from three littermate animals for each group, $P < 0.001$) (Fig. 2I and fig. S1). These results indicated that in vivo mutant HRAS–induced astrocyte areas are similar to those exhibited in vitro.

Identification and rescue of a RASopathic response in human astrocytes

Next, we conducted an unbiased transcriptional analysis with mRNA microarrays (table S1 and fig. S3) to uncover the mechanistic drivers of altered glial development and function. Accelerated gliogenesis was confirmed by the increased expression of gliogenic factors (ID1, HES1), as well as a decrease of neurogenic factors (NeuroD1, NeuroG1), transcription regulators well known to control cell identity during early differentiation (46). Other altered transcripts could generally be grouped into three major categories: Ras pathway regulation and response (SPRY2, ELK3), pro-synaptogenesis (THBS1, GPC6), and most prevalently, extracellular environment modulation (Fig. 3A and fig. S2). This latter category included small leucine-rich proteoglycans (SLRPs) (LUM, DCN, and FMOD), modifiers of heparin sulfate proteoglycans (HSPGs) (SULF1) and chondroitin sulfate proteoglycans (CSPGs) (CHSY3), as well as various supporters of matrix fibrillogenesis (POSTN, SPARC, FBLN2, and TIMP3). The predominance of extracellular environment modulation-related constituents suggests that increased matrix accumulation and stabilization may be especially promising candidate processes connecting astrocyte misdevelopment with effects upon neuronal function.

To confirm the specificity of activated HRAS signaling on this transcriptional profile, and prove competency of these cells for drug testing, we treated $HRAS^{G12S}$ astrocytes with the farnesyl transferase inhibitor FTI-277, which has high specificity for decreasing overactive HRAS activity (47). FTI-277 administered at 1 μM for 1 week was sufficient to reduce pERK and HRAS activation in $HRAS^{G12S}$ astrocytes (fig. S4). After an acute 2-week treatment of astrocytes in triplicate from 18 to 20 weeks of development from the $HRAS^{G12S}$ iPSC line 7, expression of several transcripts was reduced, including the transcription factor SNAI2 (also known as SLUG) (Fig. 3B). This acute treatment did not affect expression of transcripts that increase during normal astrocyte development from 8 to 28 weeks (THBS1, SPARC) (table S1), but acted upon those that are not developmentally regulated (POSTN, MGP, LUM, and GPC6). Because periostin was the most highly up-regulated transcript encoding an extracellular protein, we measured its concentration in astrocyte-conditioned media (ACM). We detected a decrease of extracellular periostin protein after treatment (concentration in ACM: control = 32.5 ± 1.7 ng/ml, FTI-277 treatment = 11.9 ± 3.0 ng/ml, $P < 0.001$) (Fig. 3C). SNAI2 is also regulated by activated Ras signaling and coexpressed in human cancer cells along with many mRNAs also enriched in $HRAS^{G12S}$ astrocytes (48–50). Thus, we investigated whether SNAI2 plays a role as an upstream regulator of this RASopathic phenotype. We measured the abundance of select Ras signaling–related transcripts 2 weeks after infection of astrocytes (in triplicate) with a previously described SNAI2 small interfering RNA (siRNA) lentiviral system (51). SNAI2 knockdown was sufficient to repress expression to a similar degreeasthat observed after FTI-277 treatment (Fig. 3D). Knockdown also led to a decrease of extracellular periostin

protein (concentration in ACM: shScrambled = 23.1 ± 4.4 ng/ml, shSNAI2 = 6.3 ± 1.8 ng/ml, $P = 0.0036$) (Fig. 3E). Together, these results demonstrate that mutant HRAS signaling dysregulates extracellular remodeling factors in part through a SNAI2-dependent pathway.

Early neuronal maturation promoted by RASopathic astrocytes

To investigate the consequences of RASopathic astroglial signaling upon neurons, we took advantage of purified early postnatal retinal ganglion cell (RGC) cultures because they are commonly used for detecting and assessing neuronal sensitivity to glial secreted factors (52–54). After 14 days of direct coculture, synaptic density (as measured by apposition of presynaptic marker synapsin 1 and postsynaptic marker PSD-95), but not synaptic area, was increased in cultures containing $HRAS^{G12S}$ astrocytes (synaptic density in the presence of $HRAS^{G12S}$ astrocytes: 147.7 ± 11.0% of cultures containing the same density of $HRAS^{WT}$ astrocytes, $P = 0.023$) (Fig. 4A and fig. S6). To isolate the effects of extracellular signals on neuronal outgrowth and, therefore, function, we generated indirect cocultures by adding 24-hour preconditioned ACM along with astrocytes cultured on hanging polyethylene terephthalate membranes to continuously provide ACM to RGCs. We consistently observed an increased outgrowth of primary neurites, measured as the length of β3-tubulin–labeled neurites not contacting neighboring cells, after 24 hours of exposure to glial-derived factors. The proportion of RGCs exhibiting outgrowth in $HRAS^{G12S}$ ACM conditions was not different from those in control ACM; however, the initial neurite projections were longer ($HRAS^{WT}$ = 45.8 ± 10.4 μm, $HRAS^{G12S}$ = 88.0 ± 23.4 μm, P= 0.046) (Fig. 4B).

To identity the extracellular proteins in $HRAS^{G12S}$ astrocytes affecting neural function, we performed shotgun mass spectrometry on concentrated ACM and compared protein abundance by calculating the average fold enrichment (AFE) of normalized spectral abundance factors, as previously conducted with cultured mouse astrocytes (55). Analyzing the same six samples used in the microarray analysis, we identified the 401 most highly abundant human proteins present in the ACM (table S2). Multiple proteins that were consistently detected in all lines and enriched in $HRAS^{G12S}$ astrocytes at 7 months were similar in function to those revealed in the microarray reported above, including those that play a role in extracellular matrix remodeling [DKK3, DAG1 and its interacting protein B3GN1 (56), SPARC, TIMP2, and collagens], and proteoglycans involved in synaptic plasticity [AGRIN (57), NCAN (58), and PGCB/BCAN (59)] (Fig. 4C and fig. S5).

What is the effect of increased astrocyte extracellular proteins upon neuronal function? To answer this, we confirmed an enrichment of proteoglyans by labeling *N*-acetylgalactosamines with biotin-labeled Wisteria floribunda agglutinin (WFA). WFA-binding proteins include neurocan and brevican, both enriched in $HRAS^{G12S}$ ACM. This labeling revealed more glycoproteins on the cell surface membranes of $HRAS^{G12S}$ astrocytes than on $HRAS^{WT}$ astrocytes (Fig. 4D). In vivo, WFA-binding proteins accumulate around cortical interneurons in the form of perineuronal nets (PNNs) (60, 61). PNNs determine experience-dependent critical periods of neuronal maturation and plasticity in a variety of circuits including the visual system (58, 62).

In the transgenic mouse model described above, Cre-dependent expression of a tdTomato reporter indicated that recombination to the $HRAS^{G12V}$ allele occurred nearly completely in Aldh1L1-positive astrocytes throughout the brain, but only rarely in cortical neuronal cells including parvalbumin (PV)–positive interneurons (fig. S6). Hence, we concluded that most $HRAS^{G12V}$-induced effects in the cortex are mediated by astrocytes. We compared the intensity of WFA-positive PNNs in the somatosensory cortex and the density of PV-expressing neurons to assess interneuron maturation. The intensity of WFA labeling of PNNs surrounding PV-positive neurons at p14 was increased (WFA-positive pixels: $HRAS^{G12V}$ = 193.4 ± 20.6% of $HRAS^{WT}$, $P = 0.0016$, $n = 15$ PNNs in three mice for each genotype), as well as the density of PV-positive neurons (labeled neurons per 2.25 mm^2: $HRAS^{WT}$ = 35.0 ± 3.6, $HRAS^{G12V}$ = 47.3 ± 6.1, $P = 0.0396$) (Fig. 4E). In both control and CS mice, Aldh1L1-GFP^+ glial processes were tightly associated with PNNs, with more processes observed in $HRAS^{G12V}$ astrocytes (Fig. 4E and fig. S6). Western blotting of p21 mouse cortex revealed an increased abundance of GFAP (densitometry normalized to GAPDH: $HRAS^{G12V}/HRAS^{WT}$ = 2.04 ± 0.42, P =0.021) and the PNN protein neurocan ($HRAS^{G12V}/HRAS^{WT}$ = 2.09 ± 0.49, $P = 0.030$), but not brevican, possibly reflecting differences between mouse and human astrocytes (Fig. 4F). To determine whether alterations in inhibitory circuits persisted at later stages of the critical period, we measured miniature inhibitory postsynaptic currents (mIPSCs) from layer IV pyramidal excitatory neurons that receive input from neighboring PV-positive neurons. At age p30–33, mIPSC amplitude was significantly increased in somatosensory cortex compared to controls (median: $HRAS^{WT}$ = 38.8 pA, interquartile range = 29.1 to 52.6 pA, $n = 10$ cells from two mice, 1981 mIPSCs; $HRAS^{G12V}$ = 40.6 pA, interquartile range = 31.0 to 54.5 pA, $n = 10$ cells from two mice, 2143 mIPSCs; $P < 0.001$, Wilcoxon rank sum) (fig. S6); however, the frequency of mIPSCs was unchanged ($HRAS^{WT}$ = 3.1 ± 0.51 Hz, $HRAS^{G12V}$ = 3.0 ± 0.35 Hz, $P > 0.05$).

Finally, we investigated whether the RASopathic astroglial phenotype was dependent on sensory experience by using a dark rearing (DR) paradigm starting before eye opening (day 8) and continuing into the critical period (day 19). We determined that this sensory deprivation reduced WFA labeling in both control and $HRAS^{G12V}$ visual cortex; however, $HRAS^{G12V}$ mice reared in both deprived and undeprived conditions retained substantially elevated WFA levels. Indeed, visual sensory deprivation was effective at reducing $HRAS^{G12V}$ visual cortex WFA levels similar to those of undeprived somatosensory $HRAS^{WT}$ areas (number of positive pixels: $HRAS^{WT}$ somatosensory = 10,722 ± 1443.2, $HRAS^{G12V}$ visual cortex = 12,302 ± 2959.3, not significant), and $HRAS^{G12V}$ mice still exhibited elevated WFA labeling relative to control mice with identical sensory experience (number of positive pixels: $HRAS^{WT}$ visual cortex = 4564.7 ± 978.9, $HRAS^{G12V}$ visual cortex = 12,302 ± 2959.3, P = 0.0127) (Fig. 4G). In summary, we identified potential causes (excessive extracellular signaling) and astrocyte-specific effects (enhanced or premature inhibitory synaptic strength) that may underlie cognitive deficits in human RASopathies. In astroglia, the mutation modifies extracellular mechanisms and leads to accumulation of PNNs and enhancement of PV neuron maturation and function during development (Fig. 5).

DISCUSSION

We found that expression of hyperactivated HRAS primarily in astrocytes is sufficient to alter timing of astrocyte development in a human iPSC model of astrocyte development, increase extracellular matrix signaling, and accelerate maturation of cortical interneurons in vivo. By combining human iPSC–based unbiased expression profiling with transgenic mouse modeling, we identified the mechanistic components of an intricate signaling pathway that operates at the expression, cellular, and neural circuit level. Because astrocytes can be stimulated and react in various ways during injury and disease (63,64), we sought to define a cell-intrinsic "RASopathic astrocyte" response in a CS NDD human and mouse model. First, similar to phenotypes previously detailed in mice carrying mutations in the Ras/MAPK pathway (22–27), we established that certain aspects of gliogenesis are accelerated, and cell size is increased in mutant HRAS human astrocytes in vitro. These results support the hypothesis that increased number or volume of glia may contribute to the increased brain size commonly observed in patients with RASopathies (31). The altered morphology that we observed is consistent with recent reports that FGF signaling, which acts through Ras signaling and other receptor tyrosine kinases (35), controls astrocyte complexity and morphology (65, 66). We then determined the consequences of this early Ras-specific maturation upon neuronal function. Our data support the hypothesis that the early abundance of astrocyte-secreted molecules results in an abnormal acceleration of neuronal maturation before the proper conclusion of periods of experience-dependent brain development. The increased size and proliferation of progenitors may be an underlying mechanism for the observed Ras-specific maturational effects. This altered regulation combined with intrinsic neuronal deficits may produce the decreased neurocognition and sociability observed in human subjects (20, 28).

Another major astrocyte-intrinsic phenotype that we report is an increased expression and abundance of extracellular matrix components and modulators, induced in part by the transcription factor SNAI2. Extracellular matrices are composed of various proteins including collagens, laminins, thrombospondins, HSPGs, CSPGs, and SLRPs, proteins that have diverse functions including neuronal guidance and astrocyte-induced synaptic maturation (67–69). Increased abundance of these proteins has also been associated with aging (41). Besides contributing to the basement membrane and the neural interstitial matrix, some of these extracellular components are constituents of PNNs, structures that enwrap subpopulations of neurons and affect both maturation and plasticity (70). Glia secrete various components of PNNs, including the CSPGs neurocan and brevican (60), and tightly associate with PNNs (71), yet astrocyte-regulated PNN formation, maintenance, and/or degradation have not previously been linked to NDDs. A similar dysregulation of extracellular proteins has also been described in CS fibroblasts (72), cardiomyocytes (including dysregulated chondroitin sulfate–bearing glycosaminoglycans) (73), and ameloblasts (74). The shared phenotypes among these CS cells suggest that all may be responsive to a single therapeutic strategy, although the complexity of astrocyte inter-and intracellular signaling may necessitate a cell-specific approach.

Increased extracellular signaling has the potential to disrupt various neuronal functions such as outgrowth, long-range signaling dynamics, and plasticity. Because experimental tools do

not yet exist to analyze dysfunctions of global extracellular matrix signaling, in this study, we focused on effects of astrocyte-induced early PNN formation. The accumulation of PNNs around PV interneurons is critical for closing experience-dependent periods of plasticity in various regions of the brain (7). PV expression and plasticity in the visual cortex are thought to be modulated by the presence of PNNs (75), possibly by PNN-dependent intracellular capture of OTX2 and Sema3a (76). Thus, the presence of early and abundant astrocyte-regulated extracellular signals in NDDs could not only promote early maturation of PV interneurons, but also close the window of plasticity before experience-dependent circuits are properly formed. Indeed, altered PNNs have been recently reported in several autism spectrum disorder (ASD) mouse models (77). In light of this, we propose that astrocyte Ras activity, SNAI2 expression, or extracellular matrix components are possible therapeutic targets for social and neurocognitive developmental disorders.

MATERIALS AND METHODS

Study design

The objective of this study was to compare developmental and functional phenotypes between astroglial cells of two differing HRAS genotypes: wild type or mutant. iPSC lines from three nonrelated control lines and four nonrelated CS lines $HRAS^{G12S}$ were differentiated to the astroglial lineage and subsequently assayed via multiple methods including immunostaining, RT-qPCR, microarrays, mass spectrometry, and coculture with neurons. Likewise, transgenic mice expressing either $HRAS^{WT}$ or $HRAS^{G12V}$ were compared to control littermate mice to account for genetic variation. All experiments were performed blind to genotype and/or treatment. Mice were assigned randomized numbers before genotyping for identification. The number of cell lines or animals used is given in each figure legend.

ACM preparation and mass spectrometry

Astrocytes were plated at a density of 500,000 cells per 9.6 cm^2 on cell culture–treated plastic. After attachment, medium was replaced with phenol red–free Neurobasal media plus GlutaMAX (Gibco) for 48 hours. ACM was collected and concentrated with Ultracel-3K filters (Amicon). One-dimensional liquid chromatography (1D LC), mass spectrometry, and spectral count calculations were performed by University of California, San Francisco (UCSF), Mass Spectrometry Core Facility. The normalized spectral count fractions were averaged from three $HRAS^{WT}$ lines and three $HRAS^{G12S}$ lines and divided to obtain the AFE for proteins that were detected at no less than 0.01% of total protein.

Astroglial differentiation

To induce neural differentiation, iPSC aggregates were formed for 24 hours in mTeSR1 (Stemcell Technologies) and then switched to a neural medium (39) with media exchange every other day. To promote neural induction, the small molecules SB431542 (5 μM, Stemgent) and LDN-193189 (0.25 μM, Stemgent) were added for 48 hours. On day 3, aggregates were attached to plates and cultured in neural medium for an additional week. On day 11, neuroepithelial cells were mechanically removed and kept as free-floating aggregates. On day 18, neural medium was supplemented with EGF and FGF2 (10 ng/ml

each). For select experiments, cells were treated with the addition of FTI-277 diluted in water (Sigma-Aldrich, F9803). For maturation, cells were plated as single-cell monolayers for 1 week in the presence of CNTF (10 ng/ml) followed by replating at equal densities for experimentation.

Cellular assays

Reactive oxygen species were measured using CellROX Green Reagent (Invitrogen). All samples were imaged under the same parameters, and signal intensity in each field was measured using ImageJ software. For proliferation, 0.2 μM BrdU was added in the medium for 6 or 12 hours, after which the cultures were fixed and incubated with 2 N HCl for 20 min before immunostaining. For Western blotting, cells or mouse cortical tissue was lysed in CelLytic M (Sigma-Aldrich) and protease inhibitors (Roche), boiled in SDS–polyacrylamide gel electrophoresis loading buffer plus β-mercaptoethanol for 5 min, and loaded at 30 μg per lane for human cells or 10 μg for brain lysate. Membranes were incubated with the following antibodies; p44/42 MAPK (pERK) (Cell Signaling Technology, 9102), GAPDH (Sigma-Aldrich, G8795), GFAP (Chemicon, MAB360), neurocan (R&D Systems, AF5800), and brevican (BD Biosciences, 610894). The H-Ras Activation Assay Kit (Cell Biolabs Inc.), Periostin Elisa Kit (Boster, EK0985), and Senescence β-Galactosidase Staining Kit (Cell Signaling Technologies, 9860) were used according to the manufacturers' instructions.

Electrophysiology

Acute cortical slices were made according to published protocols (78–80). Briefly, whole brains were rapidly removed from p30–33 mice, and immersed in ice-cold cutting solution consisting of the following: NaCl (87 mM), sucrose (75 mM), $NaHCO_3$ (25 mM), glucose (10 mM), MgCl2 (7 mM), KCl (2.5 mM), NaH_2PO4 (1.25 mM), and $CaCl_2$ (0.5 mM), oxygenated by bubbling with a blend of 95% O_2/5% CO_2. Parasagittal slices were made with the dorsal aspect of the brain angled down by 10° to 15°. Slices were transferred to warm (33°C) cutting solution. Recordings were performed at room temperature in oxygenated artificial cerebrospinal fluid consisting of the following: NaCl (124 mM), glucose (10 mM), KCl (2.69 mM), MgSO4 (2 mM), $CaCl_2$ (2 mM), and KH_2PO_4 (1.25 mM). Whole-cell voltage clamp recordings were made at −70 mV using glass capillaries pulled to a resistance of 2.5 to 3.5 megohms, and loaded with the following: CsCl (130 mM), Hepes (10 mM), EGTA (5 mM), $CaCl_2$ (1 mM), $MgCl_2$ (1 mM), NaCl (1 mM), QX-314 (5 mM), Na_2–ATP (adenosine 5′-triphosphate) (2 mM), and Na-GTP (guanosine 5′-triphosphate) (0.2 mM), pH 7.3, chloride-reversal potential = 0.83 mV. Neuronal firing and excitatory neurotransmission were blocked with tetrodotoxin (1 μM), 2,3-dioxo-6-nitro-1,2,3,4-tetrahydrobenzo[*f*]quinoxaline-7-sulfonamide (NBQX) (20 μM), and D,L-2-amino-5-phosphonovaleric acid (APV) (50 μM). mIPSC frequency and amplitude were measured offline using Mini Analysis (Synaptosoft).

Hippocampal organotypic slice cultures

Hippocampi were removed from p21 mice and cut using a tissue slicer (Stoelting Co.) as described (81). Cultures were maintained on 0.4-μm, 30-mm culture inserts (Millipore) in standard cell culture conditions.

Immunochemistry

Immunocytochemistry of cell cultures was performed after a 30-min fixation with ice-cold 4% paraformaldehyde or a 4-hour postfixation for immunohistochemistry of perfused brains followed by sucroseembedded cryosectioning. Samples were blocked in 0.25% Triton X-100 with 5% goat or donkey serum and labeled with the following antibodies: CD44 (BD Biosciences, 559046), S100 (Abcam, ab868), GFAP (Dako, Z0334, Chemicon, MAB360), cleaved caspase 3 (Millipore, ab3623), BrdU (Abcam, ab6326), GFP (Aves, GFP-1020), TuJ1/β3-tubulin (Covance, MMS-435P), AQP4 (Abcam, ab11026), THBS1 (Pierce, MA5-13398), synapsin 1 (Synaptic Systems, 106 103), PSD-95 (Abcam, ab2723), NeuN (Chemicon), γ-aminobutyric acid (GABA) (Sigma, A2052), and PV (Swant, PV25). Biotin-WFA (Sigma, L1516; 20 μg/ml working solution) was incubated on samples and then detected with antistreptavidin secondary fluorescent antibody (Invitrogen). To measure PNNs and Aldh1L1-GFP astrocytes, all images were acquired blindly and with the same acquisition parameters. Image analysis was conducted in ImageJ using an identical procedure for each: Positive pixels over that of background were binarized, and the number of pixels was calculated using the integrated density feature. Human astrocytes in brain slices were detected with the STEM123 antibody (Stem Cells Inc., AB-123-U-050) using a previously published staining protocol (82).

iPSC generation and confirmation

Fibroblasts were generated from skin biopsies collected by K.A.R. and L.A.W. in patients previously described (28) and expanded by culturing in Dulbecco's modified Eagle's medium + 10% fetal bovine serum for 2 to 3 weeks. Two control lines, 162D and 165D, were from healthy siblings of NF1 patients. Line 13 was generated from fibroblast line GM00498 (Coriell). Fibroblast lines were reprogrammed with nonintegrative plasmids as previously described (37). Clonal colonies displaying iPSC morphology were manually selected and subsequently cultured on a Matrigel substrate (BD Biosciences) with mTeSR1 medium (Stem Cell Technologies). To determine pluripotency, teratomas were generated via three subcutaneous injections of 100,000 dissociated iPSCs in mTeSR1/30% Matrigel into nonobese diabetic mice/severe combined immunodeficient mice (Jackson Laboratory). After 2 to 3 months, tumors were surgically removed and sections were hematoxylin and eosin–stained by the Gladstone Histology Core at UCSF. All experiments were conducted with lines between passages 10 and 30.

Microarray

RNA was purified with RNAeasy kits with on-column DNase digestion (Qiagen). RNA samples were processed, assayed, and normalized using ST1.0 Affymetrix chips by the Gladstone Genomics Core. Heat maps were generated using MultiExperiment Viewer. Functional categories were determined on the basis of examination of scientific literature. The $\log_2$ signal intensities were averaged from three $HRAS^{WT}$ and three $HRAS^{G12V}$ lines and compared using unpaired *t* tests.

Reverse transcription quantitative polymerase chain reaction

RNA was extracted from cells using TRIzol (Invitrogen) according to the manufacturer's protocol. Reverse transcription was performed using iScript RT Supermix (Bio-Rad). qPCR and melting curve analyses were performed using Sso ADV SYBR Green SMX (Bio-Rad) on a CFX96 Real-Time System (Bio-Rad). The primers used for qPCR are listed in fig. S7.

RGC coculture

RGCs were purified from P4–5 rats (Jackson Labs) as described (83). Briefly, retinas were dissociated by papain treatment and immunopanned with Thy1.1 hybridoma supernatant antibody. Indirect cocultures were generated by plating 50,000 CNTF matured astrocytes onto 1.0-μm polyethylene terephthalate (PET) hanging inserts (Millipore, PIRP12R48). For measuring synaptic puncta, the Puncta Analyzer plugin for ImageJ was used as previously described (84).

SNAI2 knockdown

Lentiviral plasmids in short hairpin RNA (shRNA) pLKO.1 vector backbones targeting SNAI2 (Addgene, Plasmid 10905: siSlug3) or a control-scrambled sequence (Addgene, Plasmid 1864: scramble shRNA) were cotransfected with shRNA lentiviral packaging vectors to generate lentiviral particles in human embryonic kidney 293 cells according to standard protocols. Viral particles were directly released into neural medium and subsequently added to astrocytes for 2 days before additional media replacements.

Statistics

For astrocyte developmental studies, SEM values were calculated using averages of each genotype, from the averages of multiple replicates (separate starting passages) from each individual line. For other experiments, unless noted, experimental data from each subject line (technical replicates) were averaged for each biological replicate. Measurements are presented as means ± SEM when multiple starting passages of each line were used, and means ± SD when one passage was used. Significance was tested using two-tailed unpaired *t* tests unless noted. When nonparametric Wilcoxon rank sum tests were used, medians are reported with interquartile ranges. In all figures, $\star P \leq 0.05$, $\star\star P \leq 0.01$, $\star\star\star P \leq 0.001$.

Transgenic mice

Mice were housed and bred at UCSF in accordance with Institutional Animal Care and Use Committee protocols. Experiments were performed after three generations of inbreeding to reduce background effects. All experimental comparisons were performed with littermate controls and in the same brain regions.

Supplementary Material

Refer to Web version on PubMed Central for supplementary material.

Acknowledgments

We thank O. Klein, A. Goodwin, and A.-C. Tien for providing the transgenic mice, M.Matthes for setting up the dark-rearing conditions, D.Lee for assistance with blind counting, and J. Dowell (University of Wisconsin-Madison) for advice on analysis of spectral counting.

Funding: Supported by the NIH New Innovator Award (1DP2OD006507), National Institute of Mental Health (R01MH099595), That Man May See, Vision Training Grant (T32 EY007120), NIH–National Eye Institute Core Grant for Vision Research (EY002162), and Research to Prevent Blindness Unrestricted Grant, and funded in part by NIH/NIAMS 5RO1AR062165 (K.A.R.) and DP2 OD007449 (L.A.W.).

REFERENCES AND NOTES

1. Perea G, Sur M, Araque A. Neuron-glia networks: Integral gear of brain function. Front Cell Neurosci. 2014; 8:378. [PubMed: 25414643]
2. Allen NJ. Astrocyte regulation of synaptic behavior. Annu Rev Cell Dev Biol. 2014; 30:439–463. [PubMed: 25288116]
3. Molofsky AV, Krencik R, Ullian EM, Tsai H-H, Deneen B, Richardson WD, Barres BA, Rowitch DH. Astrocytes and disease: A neurodevelopmental perspective. Genes Dev. 2012; 26:891–907. [PubMed: 22549954]
4. Verkhratsky A, Sofroniew MV, Messing A, deLanerolle NC, Rempe D, Rodríguez JJ, Nedergaard M. Neurological diseases as primary gliopathies: A reassessment of neurocentrism. ASN Neuro. 2012; 4:e00082. [PubMed: 22339481]
5. Zoghbi HY, Bear MF. Synaptic dysfunction in neurodevelopmental disorders associated with autism and intellectual disabilities. Cold Spring Harb Perspect Biol. 2012; 4:a009886. [PubMed: 22258914]
6. McGee A, Li G, Lu Z, Qiu S. Convergent synaptic and circuit substrates underlying autism genetic risks. Front Biol. 2014; 9:137–150.
7. Takesian AE, Hensch TK. Balancing plasticity/stability across brain development. Prog Brain Res. 2013; 207:3–34. [PubMed: 24309249]
8. Chung W-S, Clarke LE, Wang GX, Stafford BK, Sher A, Chakraborty C, Joung J, Foo LC, Thompson A, Chen C, Smith SJ, Barres BA. Astrocytes mediate synapse elimination through MEGF10 and MERTK pathways. Nature. 2013; 504:394–400. [PubMed: 24270812]
9. Wiese S, Karus M, Faissner A. Astrocytes as a source for extracellular matrix molecules and cytokines. Front Pharmacol. 2012; 3:120. [PubMed: 22740833]
10. Kanski R, van Strien ME, van Tijn P, Hol EM. A star is born: New insights into the mechanism of astrogenesis. Cell Mol Life Sci. 2014; 71:433–447. [PubMed: 23907612]
11. Sloan SA, Barres BA. Mechanisms of astrocyte development and their contributions to neurodevelopmental disorders. Curr Opin Neurobiol. 2014; 27C:75–81. [PubMed: 24694749]
12. Stipursky J, Spohr TC, Sousa VO, Gomes FCA. Neuron–astroglial interactions in cellfate commitment and maturation in the central nervous system. Neurochem Res. 2012; 37:2402–2418. [PubMed: 22614925]
13. Zeidán-Chuliá F, Salmina AB, Malinovskaya NA, Noda M, Verkhratsky A, Moreira JCF. The glial perspective of autism spectrum disorders. Neurosci Biobehav Rev. 2014; 38:160–172. [PubMed: 24300694]
14. Krencik R, Ullian EM. A cellular star atlas: Using astrocytes from human pluripotent stem cells for disease studies. Front Cell Neurosci. 2013; 7:25. [PubMed: 23503583]
15. Krencik R, Zhang S-C. Stem cell neural differentiation: A model for chemical biology. Curr Opin Chem Biol. 2006; 10:592–597. [PubMed: 17046316]
16. Kondo T, Asai M, Tsukita K, Kutoku Y, Ohsawa Y, Sunada Y, Imamura K, Egawa N, Yahata N, Okita K, Takahashi K, Asaka I, Aoi T, Watanabe A, Watanabe K, Kadoya C, Nakano R, Watanabe D, Maruyama K, Hori O, Hibino S, Choshi T, Nakahata T, Hioki H, Kaneko T, Naitoh M, Yoshikawa K, Yamawaki S, Suzuki S, Hata R, Ueno S, Seki T, Kobayashi K, Toda T, Murakami K, Irie K, Klein WL, Mori H, Asada T, Takahashi R, Iwata N, Yamanaka S, Inoue H.

Modeling Alzheimer's disease with iPSCs reveals stress phenotypes associated with intracellular Aβ and differential drug responsiveness. Cell Stem Cell. 2013; 12:487–496. [PubMed: 23434393]

17. Serio A, Bilican B, Barmada SJ, Ando DM, Zhao C, Siller R, Burr K, Haghi G, Story D, Nishimura AL, Carrasco MA, Phatnani HP, Shum C, Wilmut I, Maniatis T, Shaw CE, Finkbeiner S, Chandran S. Astrocyte pathology and the absence of non-cell autonomy in an induced pluripotent stem cell model of TDP-43 proteinopathy. Proc Natl Acad Sci USA. 2013; 110:4697–4702. [PubMed: 23401527]
18. Chen C, Jiang P, Xue H, Peterson SE, Tran HT, McCann AE, Parast MM, Li S, Pleasure DE, Laurent LC, Loring JF, Liu Y, Deng W. Role of astroglia in Down's syndrome revealed by patient-derived human-induced pluripotent stem cells. Nat Commun. 2014; 5:4430. [PubMed: 25034944]
19. Williams EC, Zhong X, Mohamed A, Li R, Liu Y, Dong Q, Ananiev GE, Mok JC, Lin BR, Lu J, Chiao C, Cherney R, Li H, Zhang SC, Chang Q. Mutant astrocytes differentiated from Rett syndrome patients-specific iPSCs have adverse effects on wild type neurons. Hum Mol Genet. 2014; 23:2968–2980. [PubMed: 24419315]
20. Tidyman WE, Rauen KA. The RASopathies: Developmental syndromes of Ras/MAPK pathway dysregulation. Curr Opin Genet Dev. 2009; 19:230–236. [PubMed: 19467855]
21. Zenker M. Clinical manifestations of mutations in RAS and related intracellular signal transduction factors. Curr Opin Pediatr. 2011; 23:443–451. [PubMed: 21750428]
22. Gauthier AS, Furstoss O, Araki T, Chan R, Neel BG, Kaplan DR, Miller FD. Control of CNS cell-fate decisions by SHP-2 and its dysregulation in Noonan syndrome. Neuron. 2007; 54:245–262. [PubMed: 17442246]
23. Hegedus B, Dasgupta B, Shin JE, Emnett RJ, Hart-Mahon EK, Elghazi L, Bernal-Mizrachi E, Gutmann DH. Neurofibromatosis-1 regulates neuronal and glial cell differentiation from neuroglial progenitors in vivo by both cAMP- and Ras-dependent mechanisms. Cell Stem Cell. 2007; 1:443–457. [PubMed: 18371380]
24. Paquin A, Hordo C, Kaplan DR, Miller FD. Costello syndrome H-Ras alleles regulate cortical development. Dev Biol. 2009; 330:440–451. [PubMed: 19371735]
25. Tien A-C, Tsai H-H, Molofsky AV, McMahon M, Foo LC, Kaul A, Dougherty JD, Heintz N, Gutmann DH, Barres BA, Rowitch DH. Regulated temporal-spatial astrocyte precursor cell proliferation involves BRAF signalling in mammalian spinal cord. Development. 2012; 139:2477–2487. [PubMed: 22675209]
26. Li X, Newbern JM, Wu Y, Morgan-Smith M, Zhong J, Charron J, Snider WD. MEK is a key regulator of gliogenesis in the developing brain. Neuron. 2012; 75:1035–1050. [PubMed: 22998872]
27. Zhu Y, Harada T, Liu L, Lush ME, Guignard F, Harada C, Burns DK, Bajenaru ML, Gutmann DH, Parada LF. Inactivation of NF1 in CNS causes increased glial progenitor proliferation and optic glioma formation. Development. 2005; 132:5577–5588. [PubMed: 16314489]
28. Adviento B, Corbin IL, Widjaja F, Desachy G, Enrique N, Rosser T, Risi S, Marco EJ, Hendren RL, Bearden CE, Rauen KA, Weiss LA. Autism traits in the RASopathies. J Med Genet. 2013; 51:10–20. [PubMed: 24101678]
29. Kratz CP, Niemeyer CM, Zenker M. An unexpected new role of mutant Ras: Perturbation of human embryonic development. J Mol Med. 2007; 85:227–235. [PubMed: 17211612]
30. Alfieri P, Piccini G, Caciolo C, Perrino F, Gambardella ML, Mallardi M, Cesarini L, Leoni C, Leone D, Fossati C, Selicorni A, Digilio MC, Tartaglia M, Mercuri E, Zampino G, Vicari S. Behavioral profile in RASopathies. Am J Med Genet A. 2014; 164A:934–942. [PubMed: 24458522]
31. Gripp KW, Hopkins E, Doyle D, Dobyns WB. High incidence of progressive postnatal cerebellar enlargement in Costello syndrome: Brain overgrowth associated with HRAS mutations as the likely cause of structural brain and spinal cord abnormalities. Am J Med Genet A. 2010; 152A:1161–1168. [PubMed: 20425820]
32. Costello JM. A new syndrome: Mental subnormality and nasal papillomata. Aust Paediatr J. 1977; 13:114–118. [PubMed: 907573]

33. Gripp KW, Lin AE. Costello syndrome: A Ras/mitogen activated protein kinase pathway syndrome (rasopathy) resulting from HRAS germline mutations. Genet Med. 2012; 14:285–292. [PubMed: 22261753]
34. Schubbert S, Shannon K, Bollag G. Hyperactive Ras in developmental disorders and cancer. Nat Rev Cancer. 2007; 7:295–308. [PubMed: 17384584]
35. Downward J. Targeting RAS signalling pathways in cancer therapy. Nat Rev Cancer. 2003; 3:11–22. [PubMed: 12509763]
36. Zampino G, Pantaleoni F, Carta C, Cobellis G, Vasta I, Neri C, Pogna EA, De Feo E, Delogu A, Sarkozy A, Atzeri F, Selicorni A, Rauen KA, Cytrynbaum CS, Weksberg R, Dallapiccola B, Ballabio A, Gelb BD, Neri G, Tartaglia M. Diversity, parental germline origin, and phenotypic spectrum of de novo HRAS missense changes in Costello syndrome. Hum Mutat. 2007; 28:265–272. [PubMed: 17054105]
37. Okita K, Matsumura Y, Sato Y, Okada A, Morizane A, Okamoto S, Hong H, Nakagawa M, Tanabe K, Tezuka K, Shibata T, Kunisada T, Takahashi M, Takahashi J, Saji H, Yamanaka S. A more efficient method to generate integration-free human iPS cells. Nat Methods. 2011; 8:409–412. [PubMed: 21460823]
38. Krencik R, Weick JP, Liu Y, Zhang Z-J, Zhang S-C. Specification of transplantable astroglial subtypes from human pluripotent stem cells. Nat Biotechnol. 2011; 29:528–534. [PubMed: 21602806]
39. Krencik R, Zhang SC. Directed differentiation of functional astroglial subtypes from human pluripotent stem cells. Nat Protoc. 2011; 6:1710–1717. [PubMed: 22011653]
40. Sosunov AA, Wu X, Tsankova NM, Guilfoyle E, McKhann GM II, Goldman JE. Phenotypic heterogeneity and plasticity of isocortical and hippocampal astrocytes in the human brain. J Neurosci. 2014; 34:2285–2298. [PubMed: 24501367]
41. Sprenger CC, Plymate SR, Reed MJ. Aging-related alterations in the extracellular matrix modulate the microenvironment and influence tumor progression. Int J Cancer. 2010; 127:2739–2748. [PubMed: 21351253]
42. Santoriello C, Deflorian G, Pezzimenti F, Kawakami K, Lanfrancone L, d'Adda di Fagagna F, Mione M. Expression of H-RASV12 in a zebrafish model of Costello syndrome causes cellular senescence in adult proliferating cells. Dis Model Mech. 2009; 2:56–67. [PubMed: 19132118]
43. Niihori T, Aoki Y, Okamoto N, Kurosawa K, Ohashi H, Mizuno S, Kawame H, Inazawa J, Ohura T, Arai H, Nabatame S, Kikuchi K, Kuroki Y, Miura M, Tanaka T, Ohtake A, Omori I, Ihara K, Mabe H, Watanabe K, Niijima S, Okano E, Numabe H, Matsubara Y. HRAS mutants identified in Costello syndrome patients can induce cellular senescence: Possible implications for the pathogenesis of Costello syndrome. J Hum Genet. 2011; 56:707–715. [PubMed: 21850009]
44. Das MM, Svendsen CN. Astrocytes show reduced support of motor neurons with aging that is accelerated in a rodent model of ALS. Neurobiol Aging. 2015; 36:1130–1139. [PubMed: 25443290]
45. Chen X, Mitsutake N, LaPerle K, Akeno N, Zanzonico P, Longo VA, Mitsutake S, Kimura ET, Geiger H, Santos E, Wendel HG, Franco A, Knauf JA, Fagin JA. Endogenous expression of $Hras^{G12V}$ induces developmental defects and neoplasms with copy number imbalances of the oncogene. Proc Natl Acad Sci USA. 2009; 106:7979–7984. [PubMed: 19416908]
46. Imayoshi I, Kageyama R. bHLH factors in self-renewal, multipotency, and fate choice of neural progenitor cells. Neuron. 2014; 82:9–23. [PubMed: 24698265]
47. Lerner EC, Qian Y, Blaskovich MA, Fossum RD, Vogt A, Sun J, Cox AD, Der CJ, Hamilton AD, Sebti SM. Ras *CAAX* peptidomimetic FTI-277 selectively blocks oncogenic Ras signaling by inducing cytoplasmic accumulation of inactive Ras-Raf complexes. J Biol Chem. 1995; 270:26802–26806. [PubMed: 7592920]
48. Anastassiou D, Rumjantseva V, Cheng W, Huang J, Canoll PD, Yamashiro DJ, Kandel JJ. Human cancer cells express Slug-based epithelial-mesenchymal transition gene expression signature obtained in vivo. BMC Cancer. 2011; 11:529. [PubMed: 22208948]
49. Yang HW, Menon LG, Black PM, Carroll RS, Johnson MD. SNAI2/Slug promotes growth and invasion in human gliomas. BMC Cancer. 2010; 10:301. [PubMed: 20565806]

50. Wang Y, Ngo VN, Marani M, Yang Y, Wright G, Staudt LM, Downward J. Critical role for transcriptional repressor Snail2 in transformation by oncogenic RAS in colorectal carcinoma cells. Oncogene. 2010; 29:4658–4670. [PubMed: 20562906]
51. Gupta PB, Kuperwasser C, Brunet J-P, Ramaswamy S, Kuo W-L, Gray JW, Naber SP, Weinberg RA. The melanocyte differentiation program predisposes to metastasis after neoplastic transformation. Nat Genet. 2005; 37:1047–1054. [PubMed: 16142232]
52. Allen NJ, Bennett ML, Foo LC, Wang GX, Chakraborty C, Smith SJ, Barres BA. Astrocyte glypicans 4 and 6 promote formation of excitatory synapses via GluA1 AMPA receptors. Nature. 2012; 486:410–414. [PubMed: 22722203]
53. Christopherson KS, Ullian EM, Stokes CC, Mullowney CE, Hell JW, Agah A, Lawler J, Mosher DF, Bornstein P, Barres BA. Thrombospondins are astrocyte-secreted proteins that promote CNS synaptogenesis. Cell. 2005; 120:421–433. [PubMed: 15707899]
54. Kucukdereli H, Allen NJ, Lee AT, Feng A, Ozlu MI, Conatser LM, Chakraborty C, Workman G, Weaver M, Sage EH, Barres BA, Eroglu C. Control of excitatory CNS synaptogenesis by astrocyte-secreted proteins Hevin and SPARC. Proc Natl Acad Sci USA. 2011; 108:E440–E449. [PubMed: 21788491]
55. Dowell JA, Johnson JA, Li L. Identification of astrocyte secreted proteins with a combination of shotgun proteomics and bioinformatics. J Proteome Res. 2009; 8:4135–4343. [PubMed: 19469553]
56. Buysse K, Riemersma M, Powell G, van Reeuwijk J, Chitayat D, Roscioli T, Kamsteeg E-J, van den Elzen C, van Beusekom E, Blaser S, Babul-Hirji R, Halliday W, Wright GJ, Stemple DL, Lin YY, Lefeber DJ, van Bokhoven H. Missense mutations in β-1,3-*N*-acetylglucosaminyltransferase 1 (*B3GNT1*) cause Walker-Warburg syndrome. Hum Mol Genet. 2013; 22:1746–1754. [PubMed: 23359570]
57. Daniels MP. The role of agrin in synaptic development, plasticity and signaling in the central nervous system. Neurochem Int. 2012; 61:848–853. [PubMed: 22414531]
58. Pizzorusso T, Medini P, Berardi N, Chierzi S, Fawcett JW, Maffei L. Reactivation of ocular dominance plasticity in the adult visual cortex. Science. 2002; 298:1248–1251. [PubMed: 12424383]
59. Frischknecht R, Seidenbecher CI. Brevican: A key proteoglycan in the perisynaptic extracellular matrix of the brain. Int J Biochem Cell Biol. 2012; 44:1051–1054. [PubMed: 22537913]
60. Bandtlow CE, Zimmermann DR. Proteoglycans in the developing brain: New conceptual insights for old proteins. Physiol Rev. 2000; 80:1267–1290. [PubMed: 11015614]
61. Faissner A, Pyka M, Geissler M, Sobik T, Frischknecht R, Gundelfinger ED, Seidenbecher C. Contributions of astrocytes to synapse formation and maturation—Potential functions of the perisynaptic extracellular matrix. Brain Res Rev. 2010; 63:26–38. [PubMed: 20096729]
62. Ye Q, Miao Q-L. Experience-dependent development of perineuronal nets and chondroitin sulfate proteoglycan receptors in mouse visual cortex. Matrix Biol. 2013; 32:352–363. [PubMed: 23597636]
63. Anderson MA, Ao Y, Sofroniew MV. Heterogeneity of reactive astrocytes. Neurosci Lett. 2013; 565:23–29. [PubMed: 24361547]
64. Burda JE, Sofroniew MV. Reactive gliosis and the multicellular response to CNS damage and disease. Neuron. 2014; 81:229–248. [PubMed: 24462092]
65. Kang K, Lee SW, Han JE, Choi JW, Song MR. The complex morphology of reactive astrocytes controlled by fibroblast growth factor signaling. Glia. 2014; 62:1328–1344. [PubMed: 24796693]
66. Stork T, Sheehan A, Tasdemir-Yilmaz OE, Freeman MR. Neuron-glia interactions through the Heartless FGF receptor signaling pathway mediate morphogenesis of *Drosophila* astrocytes. Neuron. 2014; 83:388–403. [PubMed: 25033182]
67. Jakeman LB, Williams KE, Brautigam B. In the presence of danger: The extracellular matrix defensive response to central nervous system injury. Neural Regen Res. 2014; 9:377–384. [PubMed: 24999352]
68. Clarke LE, Barres BA. Emerging roles of astrocytes in neural circuit development. Nat Rev Neurosci. 2013; 14:311–321. [PubMed: 23595014]

69. Schaefer L, Schaefer RM. Proteoglycans: From structural compounds to signaling molecules. Cell Tissue Res. 2010; 339:237–246. [PubMed: 19513755]
70. Wang D, Fawcett J. The perineuronal net and the control of CNS plasticity. Cell Tissue Res. 2012; 349:147–160. [PubMed: 22437874]
71. Derouiche A, Härtig W, Brauer K, Brückner G. Spatial relationship of lectin-labelled extracellular matrix and glutamine synthetase-immunoreactive astrocytes in rat cortical forebrain regions. J Anat. 1996; 189(Pt. 2):363–372. [PubMed: 8886958]
72. Klüppel M, Samavarchi-Tehrani P, Liu K, Wrana JL, Hinek A. *C4ST-1/CHST11*-controlled chondroitin sulfation interferes with oncogenic HRAS signaling in Costello syndrome. Eur J Hum Genet. 2012; 20:870–877. [PubMed: 22317973]
73. Hinek A, Teitell MA, Schoyer L, Allen W, Gripp KW, Hamilton R, Weksberg R, Klüppel M, Lin AE. Myocardial storage of chondroitin sulfate-containing moieties in Costello syndrome patients with severe hypertrophic cardiomyopathy. Am J Med Genet A. 2005; 133A:1–12. [PubMed: 15637729]
74. Goodwin AF, Tidyman WE, Jheon AH, Sharir A, Zheng X, Charles C, Fagin JA, McMahon M, Diekwisch TG, Ganss B, Rauen KA, Klein OD. Abnormal Ras signaling in Costello syndrome (CS) negatively regulates enamel formation. Hum Mol Genet. 2014; 23:682–692. [PubMed: 24057668]
75. Yamada J, Ohgomori T, Jinno S. Perineuronal nets affect parvalbumin expression in GABAergic neurons of the mouse hippocampus. Eur J Neurosci. 2015; 41:368–378. [PubMed: 25411016]
76. Miyata S, Kitagawa H. Mechanisms for modulation of neural plasticity and axon regeneration by chondroitin sulphate. J Biochem. 2015; 157:13–22. [PubMed: 25381371]
77. Gogolla N, Takesian AE, Feng G, Fagiolini M, Hensch TK. Sensory integration in mouse insular cortex reflects GABA circuit maturation. Neuron. 2014; 83:894–905. [PubMed: 25088363]
78. Eggermann E, Jonas P. How the 'slow' Ca^{2+} buffer parvalbumin affects transmitter release in nanodomain-coupling regimes. Nat Neurosci. 2012; 15:20–22. [PubMed: 22138646]
79. Perea G, Yang A, Boyden ES, Sur M. Optogenetic astrocyte activation modulates response selectivity of visual cortex neurons in vivo. Nat Commun. 2014; 5:3262. [PubMed: 24500276]
80. Davie JT, Kole MHP, Letzkus JJ, Rancz EA, Spruston N, Stuart GJ, Häusser M. Dendritic patch-clamp recording. Nat Protoc. 2006; 1:1235–1247. [PubMed: 17406407]
81. Opitz-Araya X, Barria A. Organotypic hippocampal slice cultures. J Vis Exp. 2011:e2462.
82. Gogolla N, Galimberti I, DePaola V, Caroni P. Staining protocol for organotypic hippocampal slice cultures. Nat Protoc. 2006; 1:2452–2456. [PubMed: 17406491]
83. Winzeler A, Wang JT. Purification and culture of retinal ganglion cells from rodents. Cold Spring Harb Protoc. 2013; 2013:643–652. [PubMed: 23818667]
84. Ippolito DM, Eroglu C. Quantifying synapses: An immunocytochemistry-based assay to quantify synapse number. J Vis Exp. 2010:2270. [PubMed: 21113117]

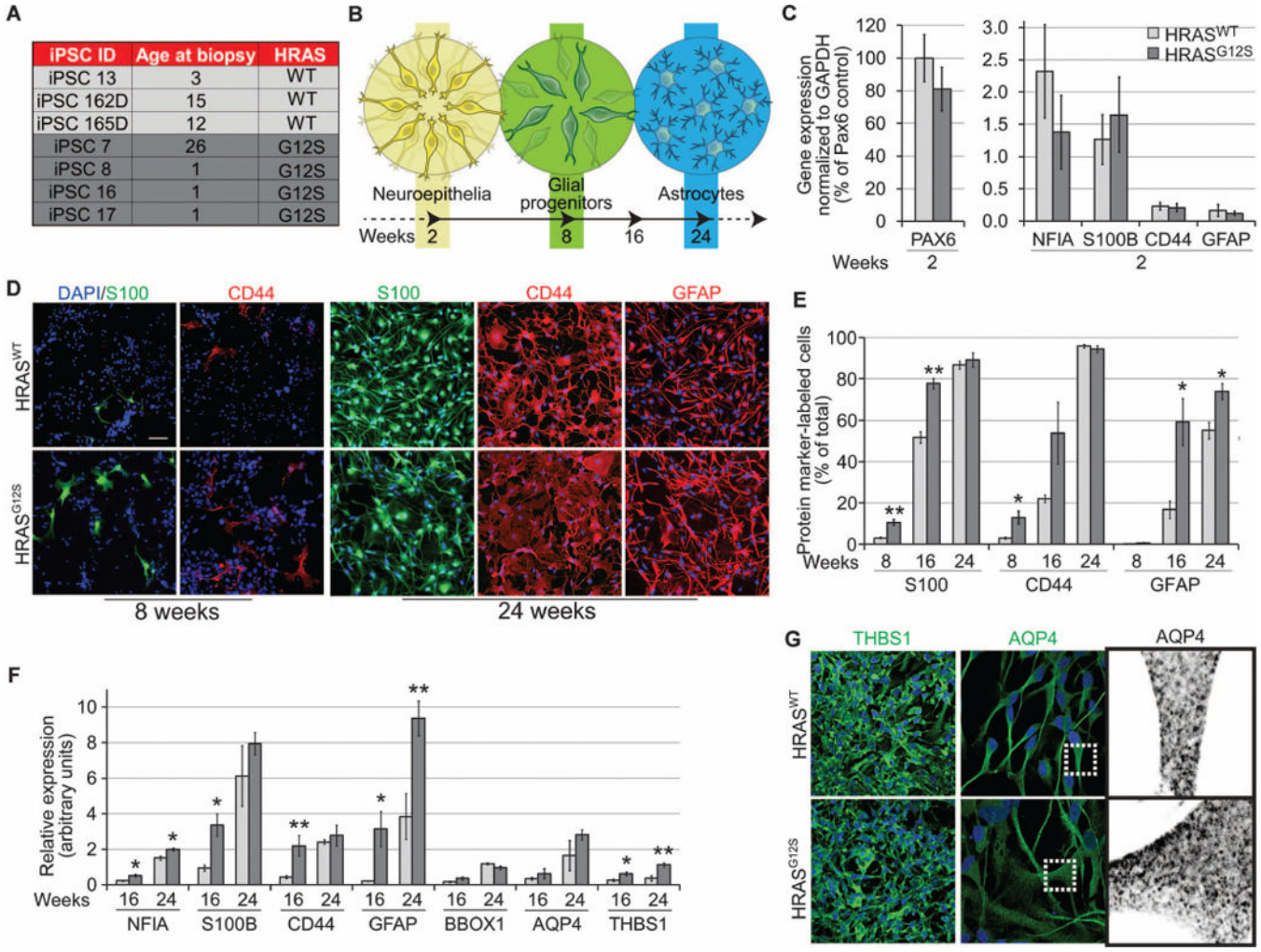

Fig. 1. Precocious Ras-dependent astroglial maturation of CS-iPSCs

(**A** to **C**) Neuroepithelial development in three wild-type (WT) and four G12S iPSC lines. (**D** and **E**) Time course of astroglial development was measured by comparing the percent of cells in $HRAS^{WT}$ lines ($n = 3$) and $HRAS^{G12S}$ lines ($n = 4$) expressing astroglial progenitor–associated markers S100 (week 8, $P = 0.007$; week 16, $P = 0.0023$) and CD44 (week 8, $P = 0.0462$), as well as the astroglial marker GFAP (week 16, $P = 0.025$; week 24, $P = 0.0274$). (**F**) Reverse transcription quantitative polymerase chain reaction (RT-qPCR) measurements of relative expression ($n = 3$ for each genotype) of astrocyte markers NFIA (week 16, $P = 0.0279$; week 24, $P = 0.0404$), S100B (week 16, $P = 0.0209$), CD44 (week 16, $P = 0.0065$), GFAP (week 16, $P = 0.0413$; week 24, $P = 0.0161$), and THBS1 (week 16, $P = 0.0484$; week 24, $P = 0.0014$). (**G**) Confocal imaging of THBS1- and AQP4-labeled astrocytes in all lines by 28 weeks. White box, magnified view. Scale bar, 50 mm. Data are displayed as means ± SEM in (C) and (E), and means ± SD in (F). GAPDH, glyceraldehyde-3-phosphate dehydrogenase; DAPI, 4′,6-diamidino-2-phenylindole.

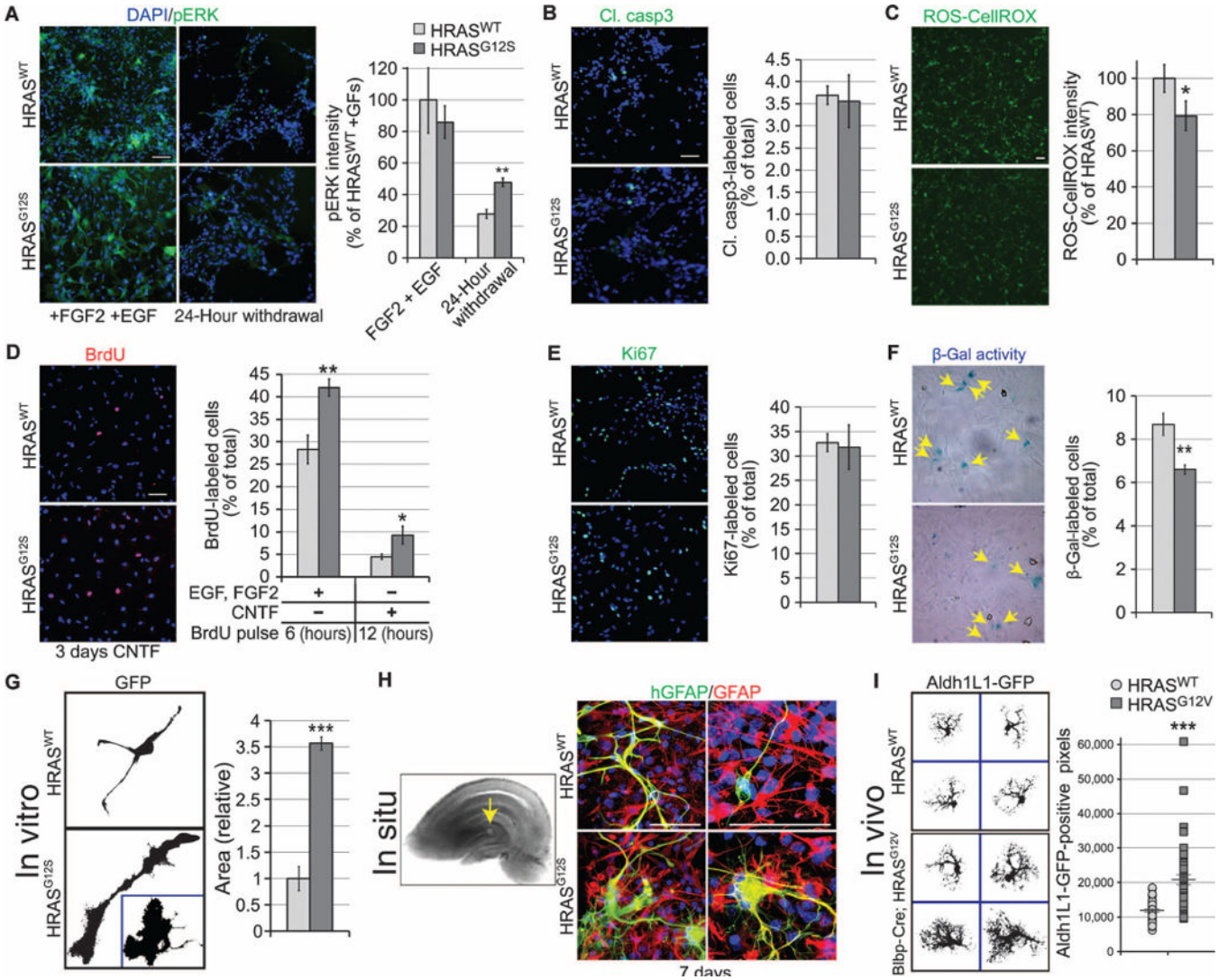

Fig. 2. Phenotypic changes induced by mutant HRAS in astrocytes

(**A**) pERK-labeled cells in HRAS^{WT} (n = 3) and HRAS^{G12S} (n = 3) cells (24-hour withdrawal, P = 0.006). (**B**) Apoptosis was determined in HRAS^{WT} lines (n = 3) and HRAS^{G12S} lines (n = 3) by assessing cleaved caspase 3 labeling (Cl. casp3). (**C**) Oxidative stress was determined by ROS-CellROX intensity in HRAS^{WT} lines (n = 3) and HRAS^{G12S} lines (n = 3, P = 0.0318). (**D**) BrdU labeling measurements for the indicated times after uptake as a marker of proliferation (in the presence of EGF and FGF2, P = 0.003; with CNTF for 3 days, P = 0.0164). (**E** and **F**) Ki67-labeled cells (E) and β-galactosidase (β-gal) activity–containing cells (F) (P = 0.009) after 8 days in the presence of CNTF. (**G**) Relative cell area measured by viral-mediated GFP expression in the presence of EGF and FGF2 (n = 3 for each group, 30 cells each; P = 0.0006). (**H**) Yellow arrow, engraftment site of a human astrosphere into a hippocampal slice culture. HRAS^{G12S}-induced morphological complexity was maintained in hippocampal slice cultures. (**I**) Size comparison of Aldh1L1-GFP–positive astrocytes in p21 HRAS^{WT} and HRAS^{G12V} mouse somatosensory cortex (n = 45

cells from three mice for each; $P = 0.0001$). Scale bar, 50 μm. Data are displayed as means ± SD. hGFAP, human GFAP.

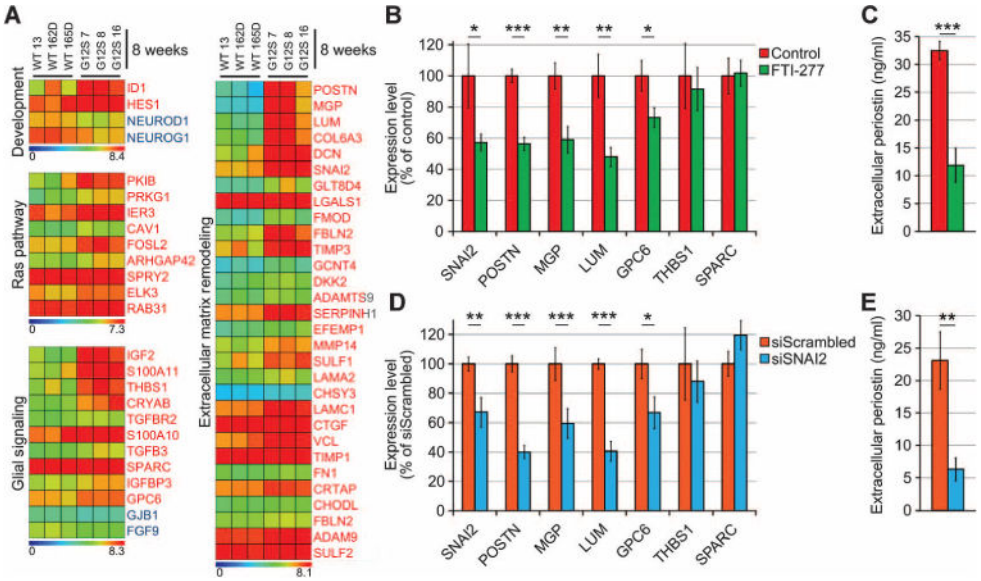

Fig. 3. Altered transcript expression caused by overactivated Ras signaling is reversed by knockdown of SNAI2

(**A**) Heat maps of select microarray signals at 8 weeks show consistent increases in multiple functional categories ($P \leq 0.05$, one-tailed *t* test) in the order from highest up-regulated on average. (**B**) Gene expression was compared in $HRAS^{G12S}$-expressing cells in the presence or absence of FTI-277 from 18 to 20 weeks of development ($n = 3$ for each group) (SNAI2, $P = 0.0245$; POSTN, $P = 0.0002$; MGP, $P = 0.004$; LUM, $P = 0.0041$; GPC6, $P = 0.0167$). (**C**) Extracellular periostin was also measured ($P = 0.0005$). (**D** and **E**) Effect of 2 weeks of SNAI2 knockdown compared against a scrambled siRNA sequence was measured in week 20 $HRAS^{G12S}$-expressing cells ($n = 3$ for each group) (D) by expression of the same set of genes (SNAI2, $P = 0.0063$; POSTN, $P = 0.0001$; MGP, $P = 0.01$; LUM, $P = 0.0002$; GPC6, $P = 0.0175$) and (E) by measuring the concentration of extracellular periostin ($P = 0.0037$). Data are displayed as means ± SD.

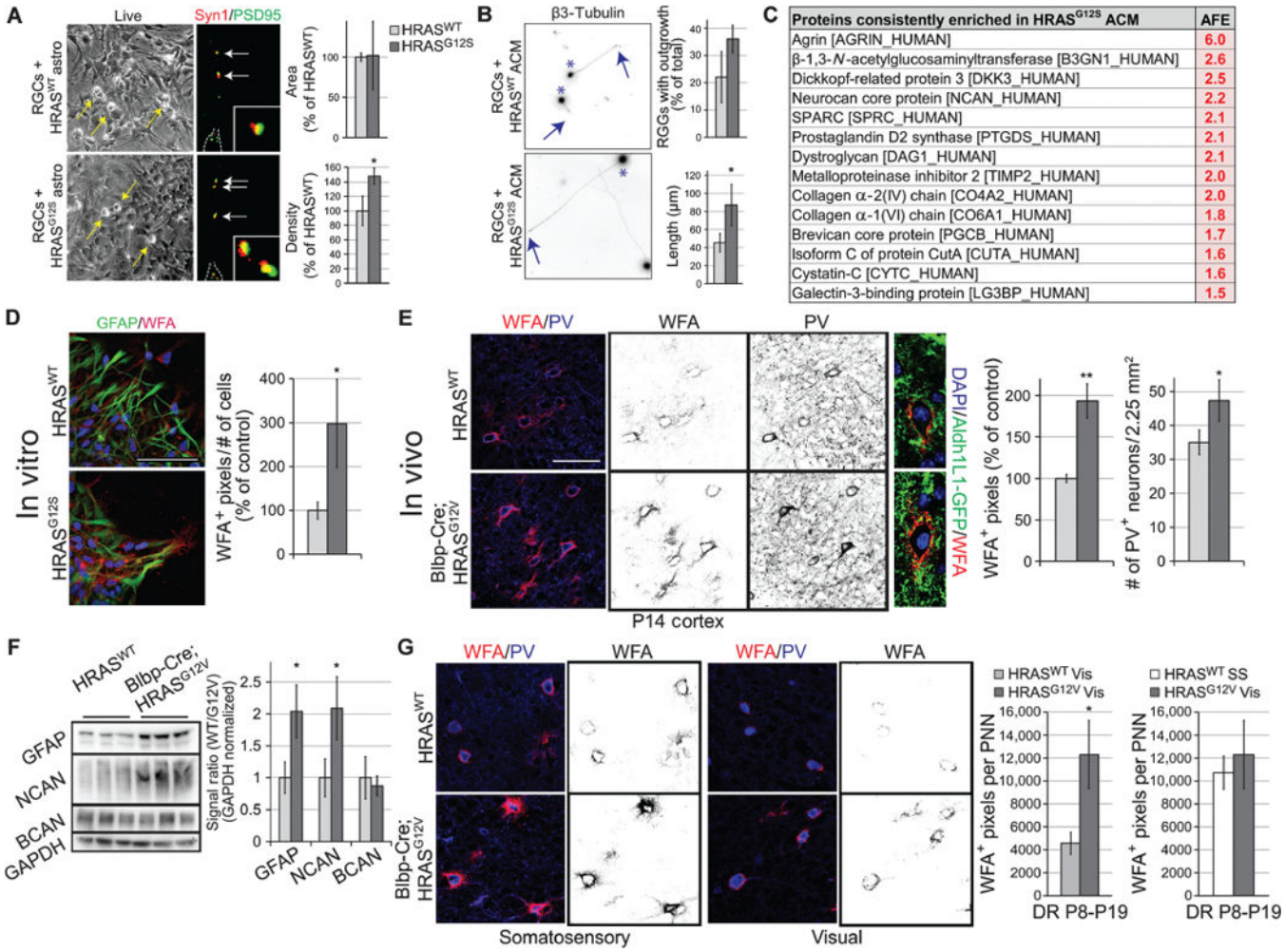

Proteins consistently enriched in HRAS^{G12S} ACM	AFE
Agrin [AGRIN_HUMAN]	6.0
β-1,3-*N*-acetylglucosaminyltransferase [B3GN1_HUMAN]	2.6
Dickkopf-related protein 3 [DKK3_HUMAN]	2.5
Neurocan core protein [NCAN_HUMAN]	2.2
SPARC [SPRC_HUMAN]	2.1
Prostaglandin D2 synthase [PTGDS_HUMAN]	2.1
Dystroglycan [DAG1_HUMAN]	2.1
Metalloproteinase inhibitor 2 [TIMP2_HUMAN]	2.0
Collagen α-2(IV) chain [CO4A2_HUMAN]	2.0
Collagen α-1(VI) chain [CO6A1_HUMAN]	1.8
Brevican core protein [PGCB_HUMAN]	1.7
Isoform C of protein CutA [CUTA_HUMAN]	1.6
Cystatin-C [CYTC_HUMAN]	1.6
Galectin-3-binding protein [LG3BP_HUMAN]	1.5

Fig. 4. Enhanced extracellular signaling by HRAS mutant astroglial cells

(**A**) Effect of coculture of RGCs with either HRAS^{WT} or HRAS^{G12S} astrocytes (n = 3 for each genotype) on synapse area and density, as measured by the relative value of apposed of pre- and postsynaptic markers Syn1 and PSD-95 (P = 0.023). Yellow arrows, RGCs; white arrows, synapses; inset, magnified example. (**B**) Neurite length was measured 24 hours after RGCs were exposed to ACM and astrocyte-containing inserts from HRAS^{WT} or HRAS^{G12S} astrocytes (n = 3 for each, P = 0.023). Asterisks, cell bodies; arrows, growth cones. (**C**) Listing of proteins found to be overabundant in HRAS^{G12S} ACM as determined by AFE over HRAS^{WT} (n = 3 for each). (**D**) Glycoprotein-containing extracellular matrix on the Surface of HRAS^{WT} and HRAS^{G12S} astrocytes (expressed as WFA + pixels/number of cells) (n = 3 for each group) (P = 0.0289). (**E**) Accumulation of WFA-labeled cortical PNNs in mice with astrocytic expression of HRAS^{WT} or HRAS^{G12V} (n = 3 for each) (P = 0.0016) and the density of PV-labeled cells (P = 0.0395). (**F**) Abundance of protein in p21 mouse cortex (n = 3 of each genotype) as measured by Western blotting (GFAP, P = 0.0202; NCAN, P = 0.0306). (**G**) WFA-labeled PNN intensity in visual cortex (Vis) and somatosensory cortex (SS) after DR of HRAS^{WT} or HRAS^{G12V} mice (n = 3 of each, littermates) from p8 to p19 (HRAS^{WT} Vis compared to HRAS^{G12S} Vis, P = 0.0128;

$HRAS^{WT}$ SS compared to $HRAS^{G12S}$ Vis, $P = 0.4524$). Scale bar, 50 μm. Significance was tested using unpaired t tests. Data are displayed as means ± SD.

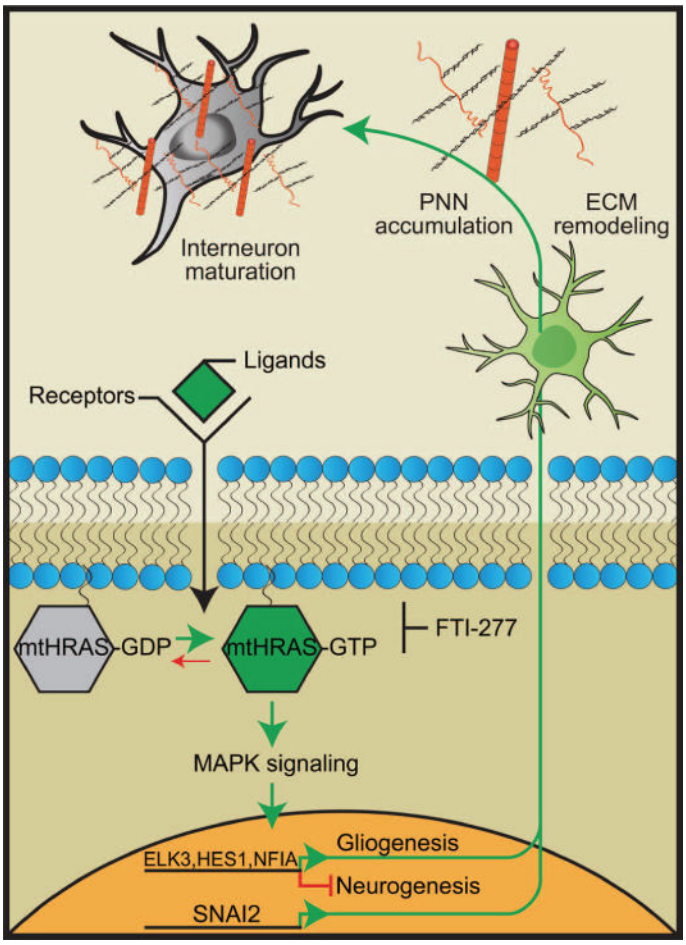

Fig. 5. Proposed model for dysfunction of RASopathic astrocytes

Overactivation of the Ras/MAPK signaling pathway in mutant HRAS (mtHRAS) astrocytes (green) results in both early Ras-specific gliogenesis and an extracellular response, which can be in part reduced by FTI-277 and SNAI2 knockdown. Subsequently, extracellular matrix remodeling occurs and leads to an experience-independent accumulation of PNNs surrounding inhibitory cortical neurons (gray), which may possibly alter critical period plasticity.